CHAPTER 5

BOOSTER ENERGY UPGRADE TO 1.4 GeV – OTHER SYSTEMS

5.1 PSB-PS LINE SEPTUM MAGNETS

In the PSB, DC septum magnets that were originally designed for 800 MeV beams, have been used for 1 GeV beams since 1986 without modification. When the PSB energy needed to be increased to 1.4 GeV it required the re-design of all PSB ejection and transfer septa because of the thermal limit of the DC magnets [1]. A single turn pulsed magnet approach which requires less energy and hence less cooling power has been adopted for the construction of these septum magnets. This way they are also less prone to erosion in the cooling circuits. To attain the required vacuum, the laminated yoke of these pulsed magnets must be baked at 200°C, despite the fact that these magnets are installed in non-bakeable accelerators. Therefore, the connecting flanges of the magnet tanks should not exceed 50°C when the magnets are being baked.

In the following paragraphs, the most important details of the modifications will be described for each component.

5.1.1 Vacuum Tanks

To reduce the risk of a leak developing during a bakeout, cylindrical tanks have been fitted with circular ultra high vacuum flanges for diameters < 200 mm and "Wheeler" flanges with copper seals for the bigger diameters (> 375 mm). The connecting flanges of the tanks to the accelerator vacuum chamber are of a conical "quick disconnect" type with aluminium seals, as standard in the CERN PS accelerators. Fig. 5.1 shows a vacuum tank containing two superposed PSB ejection septum magnets.

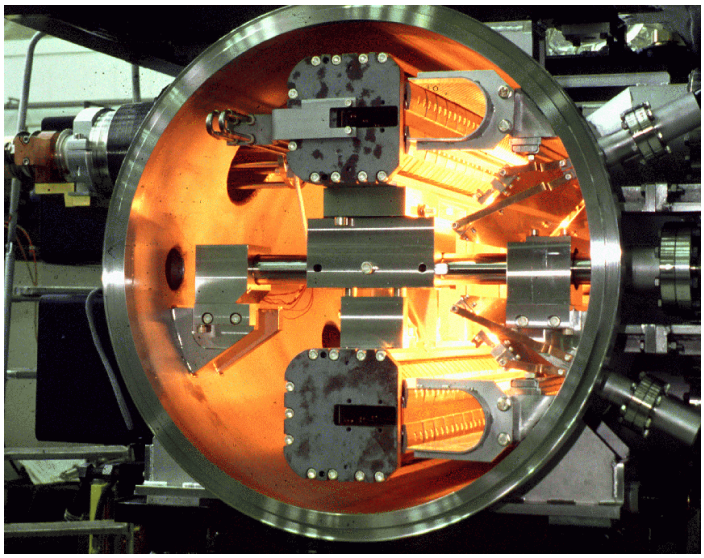

Figure 5.1: Vacuum tank containing two superposed ejection magnets.

5.1.2 Magnets

Because the new septum magnets are a pulsed, they are constructed with laminated yokes. Standard 0.35 mm thickness steel laminations with a 3% silicon content, which are insulated on both sides with a "Carlite" inorganic insulating coating have been used. This solution provides a good inter-laminar resistance and is still bakeable up to 200°C. The laminated yoke is held together in a stainless steel support by ceramic coated endplates and sits on ceramic bars, to ensure the electrical insulation between the yoke and the support.

The single-turn coils have been made of "OFHC" copper. The cooling circuit comprises two thin-walled stainless steel tubes, embedded (and brazed) in pre-machined slots in the septum conductor. This reduces erosion of the cooling circuit due to the high water speeds of up to 10 m/s. To increase the mechanical strength of the 60 mm gap septa conductors, a 0.5 mm thick stainless steel plate is brazed onto the outside of the septum conductor. To reduce the fringe field of the magnets, insulation has been eliminated between magnet yoke and septum conductor, while the return conductor of the coil is insulated with several layers of 0.06 mm and 0.12 mm thermally pre-formed "Kapton" sheet (see Fig. 5.2).

The complete magnet coil is held in the gap by clamping plates which are located outside the magnet yoke. These insulated clamps retain the septum conductor in the gap, while a spring between the septum and rear conductor applies a mechanical force on the return conductor equal to the electromechanical force at the peak current.

The springs, spaced every 45 mm, are made of beryllium copper (5% Be) suitably annealed to obtain the necessary modulus of elasticity (see Fig. 5.3).

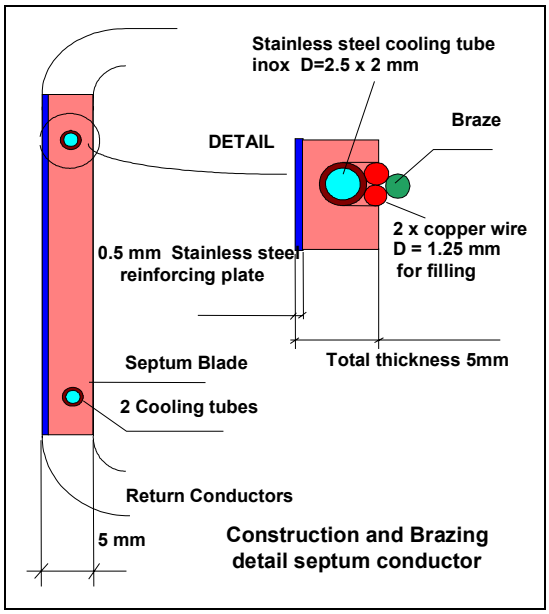

Figure 5.2: Cross section of septum conductor.

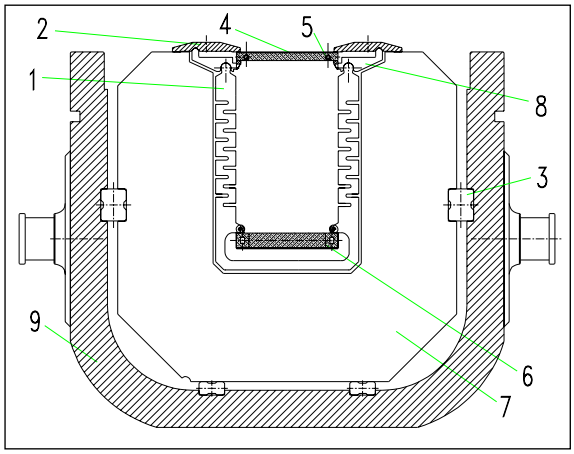

Figure 5.3: Cross section of magnet yoke assembly.
1. Damping Spring 2. Clamping Plate
3. Ceramic Support 4. Septum Conductor
5. Cooling Tube 6. Rear Conductor 7. Lamination
8. Lever 9. Stainless Steel Support.

A water-cooled coaxial power feedthrough, developed for use at 10 kA_{rms}, is used for all new pulsed septum magnets. The coaxial configuration provides the best possible symmetry in mechanical forces, (see Fig. 5.4)

5.1.3 Displacement System

All septum magnets can be moved remotely in the radial (or vertical, in the case of the septa in the transfer line) and angular directions, while their vacuum tanks remain fixed. A variable potentiometer, linked to the mechanical displacement system, provides a measurement of the position of the magnet inside the tank. The resolutions of the radial and angular systems are 0.1 mm and 0.1 mrad, respectively. For the initial installation, the magnet tank is aligned in all directions. In the event of a failure, the entire vacuum tank with septum magnet can be replaced without the need for realignment.

5.1.4 Beam Screen

All septum magnet tanks (except transfer lines) are equipped with RF beam screens for the orbiting beam. These screens ensure the continuity of the RF impedance of the vacuum tanks needed to avoid unwanted harmonics during acceleration. The beam screens are made of perforated stainless steel sheet to improve vacuum pumping speed and are linked to the connecting flanges of the tank by means of RF contacts.

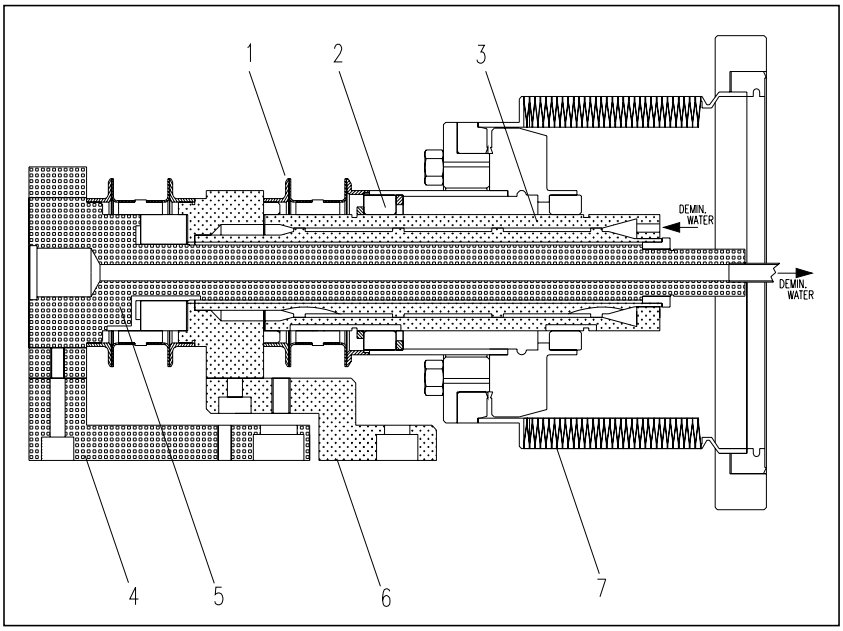

Figure 5.4: Cross section of power feedthrough. 1. Dilver / Stainless steel weld 2. Ceramic support 3. External conductor 4. Main connection 5. Central conductor 6. Main connection 7. Vacuum bellows.

5.1.5 Vacuum Equipment

The vacuum tanks are kept under vacuum with a dedicated set of ion pumps, with additional pumping provided by titanium sublimators for the tanks installed in the accelerator rings. In view of the large surface area of the magnet laminations under vacuum and the pressure level to be obtained, it is necessary to bake out the magnets before commissioning. Standard off-the-shelf infra red lamps with reflectors of electro-polished stainless steel are used inside the vacuum tank. By connecting two reflectors in series, the power consumption is reduced by a factor four, while the expected life time is dramatically increased. The temperature of the magnet is measured with ordinary Cu/Cn (Cn-Constantan) thermocouples and the control and regulation utilises standard temperature regulators.

5.1.6 Calculations

A program was used developed in house for the first rough estimation of the septum magnet parameters. To finalise the cross sectional design of the magnet a finite element based program called “FLUX2D” from Cedrat/Magsoft was used. The longitudinal design was determined using the finite element based program “OPERA3D/TOSCA” from Vector Fields, using a technique developed in house to simplify the magnet model without significant loss of precision. For mechanical and thermal calculations the finite element program ANSYS from Swanson Analysis Systems was used, while the cooling requirements were checked with the CERN package TUBE.

5.1.7 Measurement Results and Conclusions

Measurements of magnetic length of the septa confirm theoretical predictions to within 0.5% of the model. The fringe fields measured are less than 1/1000 of the gap field at a 50 mm distance from the septum conductor, or better in case of the BE.SMH (PSB ejection), where a very low fringe field was required. After a bakeout cycle, consisting of a quasi linear temperature increase to 200°C over 12 hours, a 24 hour period at 200°C and an exponential temperature decrease of approximately 48 hours, a vacuum of 6×10^{-10} to 4×10^{-9} mbar is achieved. Since the bakeout lamps are installed with reflectors, the connecting flanges of the vacuum tanks never exceed 50°C, allowing the use of aluminium seals for connecting to the accelerator vacuum chambers. For completeness, the technical specifications of the septum magnets are listed in Tab. 5.1.

Table 5.1: Technical specifications of the septum magnets.

		BESMH	BTSMV10	BTSMV20	PISMH42
$L_{eq.}$	[m]	0.95	1.00	1.00	0.57
B_0	[T]	0.354	0.569	0.525	0.689
$\int Bdl$	[Tm]	0.336	0.566	0.523	0.390
I single turn coil	[kA]	7.0	27.3	25.2	33.1
E protons	[GeV]	1.4	1.4	1.4	1.4
Deflection Angle	[mrad]	47	79	73	55
Gap height	[mm]	25	60	60	60
Gap width	[mm]	89	116	116	116
Septum Thickness	[mm]	3.8	5	5	5
Rear conductor thickness	[mm]	7.6	8.8	8.8	8.8
1/2 sine pulse width	[ms]	3.1	3.1	3.1	3.2
Water flow	[l/min]	1.9	3.5	3.5	4.25
Year of installation		1998	1999	1997	1996

5.2 PSB-PS TRANSFER LINE MAGNETS

Most of the magnets in the transfer line from the PSB to the PS had to be replaced, for two different reasons. Some of the original magnets were not laminated, thus the induced eddy currents would have hindered pulse to pulse modulation. For some other magnets, the cooling power was no longer sufficient at the higher currents necessary for 1.4 GeV operation. The new magnets are part of the Canadian in-kind contribution to the LHC project.

All the magnet yokes are laminated using low carbon steel sheets of 1.5 mm thickness stacked between non-laminated low carbon steel end plates. The coils are built from rectangular copper conductor with a circular cooling hole. The inter-turn and mass insulation is made with half-lapped glass fibre tape. The coils are vacuum impregnated using radiation resistant epoxy resin.

The BVT10 dipoles are window frame magnets with a single bedstead coil. A yoke extension block compensates the asymmetry caused by the coil head. The BVT20 magnet is similar to the BVT10, but with an aperture of twice the width and two symmetrical bedstead coils which are identical to the BVT10 coils. The DVT correction dipoles are window frame magnets with less bending power. They have two bedstead coils. The yokes of the BT.QNO quadrupoles use a “figure of eight” design. The doublet version is built from two single yokes separated by appropriate spacers. Details about the magnet design and excerpts from the construction drawings can be found in [2, 3] and the references therein.

The quadrupoles were magnetically measured at TRIUMF with a newly built rotating coil system [3] and an existing Hall probe system. The dipoles were field mapped at TRIUMF using a Hall probe system. Details of the measurements, comparisons between different measurement methods and comparisons to magnetic field calculations can be found in [2 – 5] and the references therein.

Tab. 5.2 lists the magnet characteristics. The values given for coolant flow, temperature rise and pressure drop are measured values. Higher currents are possible by increasing the inlet water pressure, the maximum permissible value being 25 bar. Tab. 5.2 also contains the coefficients $\int B\mathrm{d}l/I$, $\int G\mathrm{d}l/I$; the value for the BVT10 dipoles corresponds to the linear part up to 200 A. At the field necessary for 1.4 GeV operation, a saturation of 0.7% can be seen for this magnet (Fig. 5.5). The polynomial coefficients to describe this curve can be found in [3]. For all other magnets saturation effects are negligible at this field level. All values are averaged over a given magnet type, individual measurements for each magnet are summarised in [3].

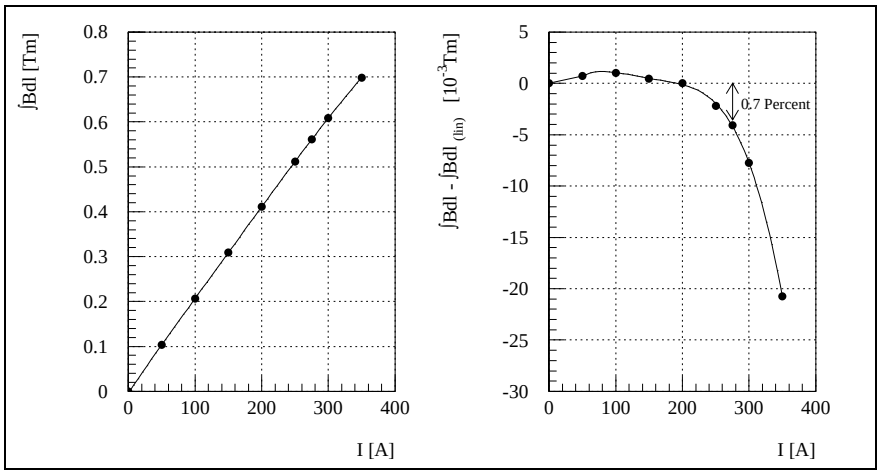

Figure 5.5: BVT10 magnetisation curve.

Table 5.2: Magnet characteristics: $\int B\mathrm{d}l$ and deflection angle correspond to the current given in this table.

		BVT10	**BVT20**	**DVT**	**BTQNO singlet**	**BTQNO doublet**
Deflection angle	[mrad]	78.5	70.0	max. 11.1	-	-
Elements		BT1.BVT10 BT4.BVT10	BT.BVT20	BT2.DVT10 BT3.DVT10 BT2.DVT20 BT3.DVT20 BT3.DVT40	BT.QNO30 BT.QNO40	BT2.QNO10 BT3.QNO10 BT2.QNO20 BT3.QNO20
Overall length	[mm]	985	980	445	590	590
Overall height	[mm]	460	460	280	500	1000
Overall width	[mm]	340	530	440	700	700
Yoke length	[mm]	800	800	250	430	430
Horizontal aperture	[mm]	62	120	102	-	-
Vertical aperture	[mm]	124	124	124	-	-
Aperture diameter	[mm]	-	-	-	150	150
Weight	[kg]	500	650	100	650	1400
Cooling flow	[l/min]	7.7	13.5	3.5	5.3	9.7
Temperature rise	[°C]	35	28	20	30	30
Pressure drop	[bar]	4.2	3.5	3.5	4.5	4.3
I (for given $\int B\mathrm{d}l$ / $\int G\mathrm{d}l$)	[A]	275	234	250	260	260
R at 20°C	[mΩ]	212.3	416.5	74.6	147.1	296.5
R at 45°C	[mΩ]	235.3	460.8	82.4	162.9	328.2
L at 100 Hz	[mH]	39.8	86.5	2.68	39.0	78.4
L at 1000 Hz	[mH]	32.6	72.7	2.16	34.3	69.2
Dissipated power	[kW]	17.8	25.3	5.2	11.0	22.0
B	[T]	0.6189	0.5476	0.1971	-	-
$\int B\mathrm{d}l$	[Tm]	0.5611	0.5003	0.07957	-	-
G	[T/m]	-	-	-	6.612	6.614
$\int G\mathrm{d}l$	[Tm/m]	-	-	-	3.082	3.082
$\int B\mathrm{d}l/I$ (BVT10: I<200A)	[Tm/A]	2.0555×10^{-3}	2.1370×10^{-3}	3.1830×10^{-4}	-	-
$\int G\mathrm{d}l/I$	[T/A]	-	-	-	1.1854×10^{-2}	1.1854×10^{-2}
Effective length	[mm]	906.6	913.6	403.8	466.1	466.0

Figs. 5.6 and 5.7 show the homogeneity of $\int B\mathrm{d}l$ of BT.BVT10#1, BT.BVT20 and BT.DVT#1. X corresponds to the horizontal, Y to the vertical direction with respect to the beam. Fig. 5.8 shows the homogeneity of G and $\int G\mathrm{d}l$ of BT.QN0#6, calculated from the harmonics measured with the rotating coil system. As a comparison, the direct measurements using a gradient flip coil system are shown.

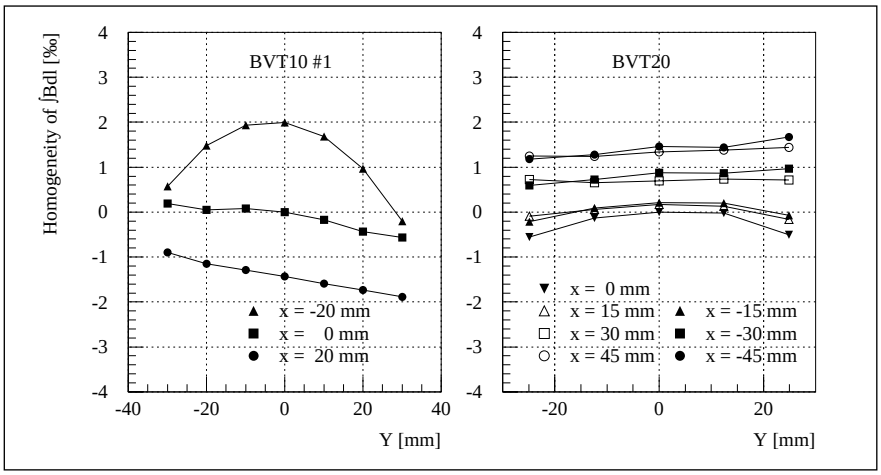

Figure 5.6: Homogeneity of $\int B\mathrm{d}l$ of BT.BVT10#1 and BT.BVT20.

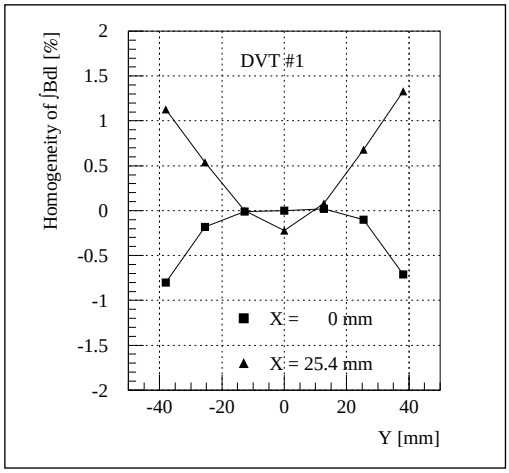

Figure 5.7: Homogeneity of $\int B\mathrm{d}l$ of BT.DVT#1.

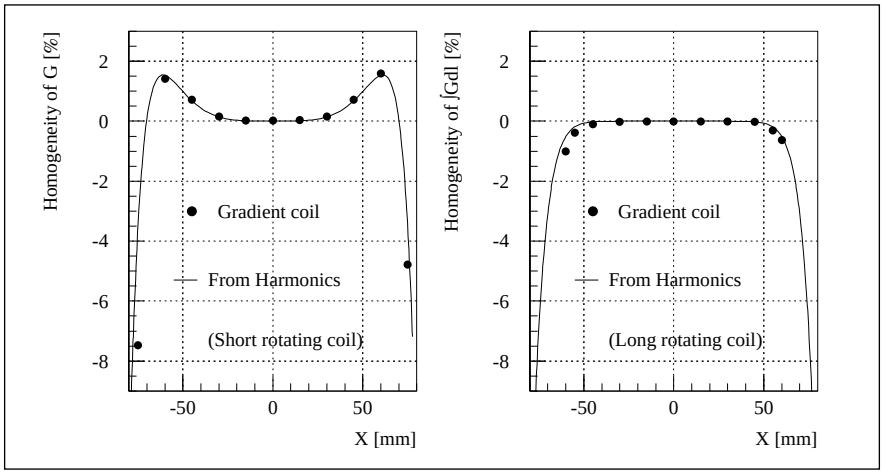

Figure 5.8: Homogeneity of G and $\int G\mathrm{d}l$ of BT.QNO#6.

5.3 FAST KICKER SYSTEMS

5.3.1 PSB Ejection BE.KFA14L1 and Recombination Kickers, BT.KFA10 and BT.KFA20

The PSB kicker magnets are used for the horizontal ejection and sequential vertical recombination of the beams from the four PSB rings into one string of bunches, which is guided to the PS. The magnets are of cellular, closed aperture, C-ferrite loaded, transmission line type; they are in the machine vacuum. Ejection and recombination magnets have different apertures to best match the beam dimensions. Given the constraints of the PSB ring and transfer line layout, the original magnets and vacuum tanks were re-used. The particularity of the original PSB kicker system configuration [6] was the insertion of the magnets between the Pulse Forming Network (PFN) and transmission cables, as sketched in Fig. 5.9 below.

The principal advantage of this extremely tailored layout is that the magnets are used in virtual short-circuit mode. The short-circuit current is provided immediately by the thyratron switch and its leading edge travels only once through the magnet. This configuration yields the fastest kick rise-time and highest kick strength for a given PFN voltage. Although the PFNs are resonantly charged in milliseconds, the crucial disadvantage of this configuration, however, is the relatively long exposure of the magnet to the PFN charging voltage, which may precipitate magnet sparking for charging voltages larger than ~ 35 kV. Because of the increase of PSB energy, (the charging voltage for the kicker pulse generators is 26% higher), this (originally air-insulated generator) configuration could not be retained, except for the second recombination kicker BT.KFA20, which operates far below the magnet voltage hold-off. This minimal cost system had other disadvantages:

- The impedance at the main thyratron switch is low (6.25 Ω), thus increasing the relative importance of unavoidable inductive mismatches present in such systems.
- Timing and transmission cable length adjustments, possible with independently powered modules, which are very effective to reduce the influence of individual magnet kick rise-time and ripple on the sum kick of the magnets, cannot be made.

During previous PSB energy upgrades, the initially effective, but cumbersome ferrite loaded pulse-steepening lines [7] (Fig. 5.9) were removed. High voltage thyratrons, vacuum feedthroughs and the magnet ferrites were upgraded (except for BT.KFA10) and all PFN and transmission cables were replaced by low loss, SF_6 pressurised high voltage cables.

For the LHC upgrade described here, the PSB kicker equipment (hardware and software) was completely replaced, except for the magnets, vacuum tanks and high voltage cables.

New, oil-insulated pulse generators using two multistage thyratrons, each capable of operating at 60 kV and in two-shot Pulse to Pulse Modulation (PPM), were developed and installed together with their associated electronics and controls for BE.KFA14L1 and BT.KFA10 [8].

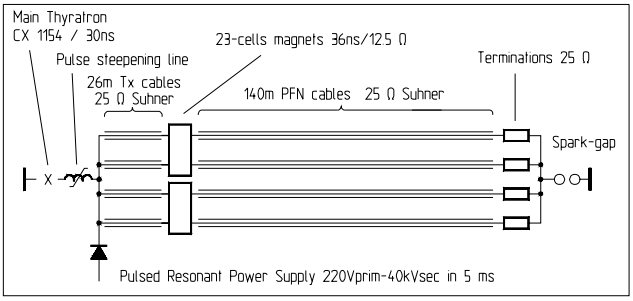

Figure 5.9: Original BT.KFA20 configuration.

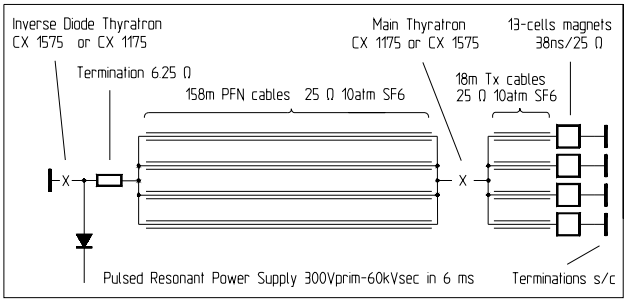

Figure 5.10: BE.KFA 14L1 (1 of 4 rings) for LHC era.

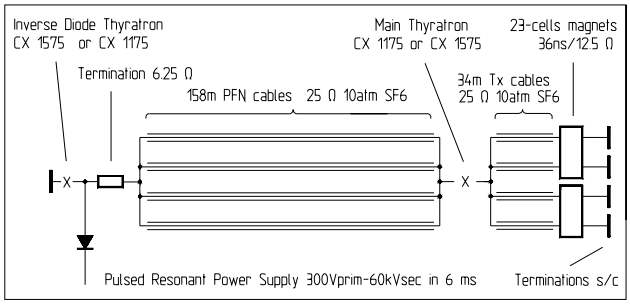

Figure 5.11: BT.KFA 10 configuration for LHC era (1 of 2 lines).

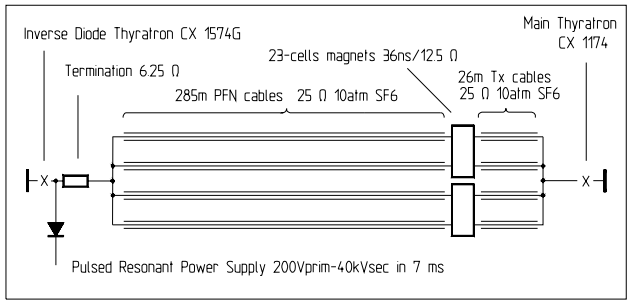

Figure 5.12: BT.KFA 20 configuration for LHC era.

These magnets are now hard short-circuited and pulsed in the more classical configurations of Figs. 5.10 and 5.11. For BT.KFA20, the new hardware developed for the above systems is also used, but the original configuration has been retained in order to achieve the short rise-time without the need of bulky requiring an artifices (Fig. 5.12).

The principal advantage of the new layout is that the short-circuited magnets (and their electrical feed-throughs) are exposed to high voltage for the minimum possible duration, largely obviating the problem of sparking. The intrinsic disadvantage of this new configuration with respect to the previous layout is that the initial switch current has to traverse the magnet twice before the total kick is established, leading to a longer rise-time (~90 ns instead of ~60 ns). However, because of the PSB harmonic number change from 5 to 2 or 1, this longer rise-time can be accepted.

Further development work on the use of saturable inductors involving the mounting of small saturable ferrite loaded inductors improved the kicker rise time. Other complications inherent in this configuration are different lengths of transmission cables to compensate for particle flight time from magnet to magnet. Much of the unavoidable flattop ripple has been reduced by adequate compensation with RC filters.

The main parameters of the PSB kickers can be found in the Tab. 5.3.

Table 5.3: PSB and PS kicker main parameters and performance (kick strengths for I_{max})

Element	No.of Gene-rators	V_{max} PFN [kV]	Magnet nominal Z_o [Ω]	Termi-nation Z_o [Ω]	Magnet I_{max} [kA]	No. of turns	Magnet Aperture w × h [mm^2]	Magnet length [mm]	Kick strength in SS/ring [Gm]	Rise-time 2-98%	Flattop length [μs]
BE.KFA14L1	4	60	25	s/c	2.4	1	115 × 70	450	775	102 ns	1.5
BT.KFA10	2	60	12.5	s/c	4.8	1	53 × 110	786	862	86 ns	1.5
BT.KFA20	1	30	12.5	s/c	2.4	1	53 × 110	786	431	80 ns	2.7
PI.KFA45	4	80	26.3	26.3/ 0	1.5 / 3	1	150 × 53	222	314.2 / 601.5	49 ns	0 - 2.6
PR.KFA71-79	12	80	15	15	2.6	1	147 × 53	221	1673	85 ns	0 - 2.1
BE.BSW14L4	1	0.5	-	-	0.765	36	141 × 144	540	946	5.25 ms	100
BE.BSW15L1	1	0.5	-	-	0.845	24	144 × 72	378	1336	5.25 ms	100
BE.BSW15L4	1	0.5	-	-	0.765	36	141 × 144	540	946	5.25 ms	100

5.3.2 PSB Ejection Dipoles

For ejection at 1.4 GeV it was necessary to increase the peak current in the bumper magnet from 500 A to 630 A. Whilst it was possible to conserve the existing magnets, their associated pulse generators were limited to 550 A peak current. In addition, the bumpers are now required to operate in PPM between 1 GeV and 1.4 GeV. In view of these new operating conditions, the need to interface to a new DSC-based control system and their advanced age, it was decided to completely replace the existing pulse generators [9].

The existing magnets, in use since 1970, were retained. BE.BSW14L4 and BE.BSW15L4 are PSB type 5 magnets, BE.BSW15L1 is a type 6 magnet. The magnets are connected in a series/parallel configuration which presents an effective impedance equivalent to that of a single magnet. This arrangement is identical for the three straight sections. Each bumper pulse generator excites four vertically superimposed magnets.

The relevant parameters for the three sections are given in Tab. 5.3. For operational purposes, I_{max} is hardware limited to 690 A for all twelve magnets.

The operating principle is based on a resonant semi-sinusoidal current discharge into the bumper magnet with a freewheel diode/inductor circuit providing a partial recharge of the primary capacitor C1. Fig. 5.13 shows a simplified electrical circuit for one bumper magnet group and its associated power supply.

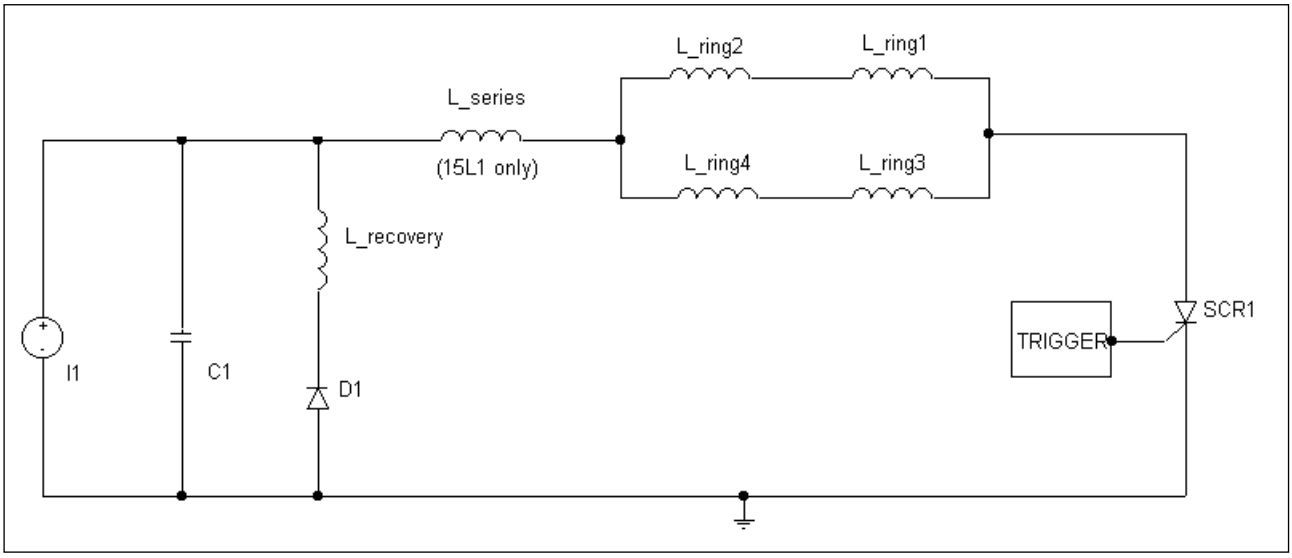

Fig. 5.13: Simplified circuit diagram of one bumper magnet group (four superimposed magnets).

C1 is charged to a voltage V by a current source I1. When the semiconductor switch, SCR1, is triggered, a resonance is excited between C1 and the magnet inductances L_ring1, L_ring2, L_ring3 and L_ring4. This slightly-damped sinusoidal current is interrupted by the opening of SCR1 at the instance of zero-crossing. Time to peak of the current pulse is 5.25 ms. The free-wheel circuit comprising D1 and L_recovery begins to conduct when the voltage on C1 goes negative; a secondary, lower-frequency resonance then occurs between L_recovery and C1 which ends when the current in D1 starts to become negative. This results in C1 completing the cycle with a positive charge, thereby reducing both the power losses and the post-cycle recharge period. An additional series inductance is required in the 15L1 circuit to compensate for the lower inductance of the type 6 magnets compared to the type 5 magnets.

5.3.3 PS Injection and Ejection Kickers

The PS injection and ejection kickers are re-used in their original configuration because they are sufficiently powerful. The PS injection Kicker PI.KFA45 works in a particular configuration (Fig. 5.14), which permits the doubling of the kick duration by short-circuiting the magnets during PPM and using timing shifts for use with ions. However, as proton injection for LHC is performed in two-batch filling mode, the previous kick rise-time had to be shortened to ~95 ns. This improvement was done with saturable inductors and matching elements, which are also very effective for the flatness and fall-time of the kick [10].

The improvement required for the PS ejection kicker KFA 71-79 (Fig. 5.15) was more dramatic. In the (now obsolete) debunching-rebunching scheme [11], 3 out of 84 bunches had to be discarded, which lead to the specified rise-time of 95 ns. However, even if 4 bunches were discarded, the resulting kick rise-time of 120 ns (0.5 - 99.5%) and flat-top stability of ± 0.5% were very difficult to achieve. Extensive computer modelling indicated that this requested performance could be obtained. Here as well, the improvement could be achieved by the introduction of saturable ferrite inductors and suitably arranged filters [12]. With the change over to the bunch splitting scheme (Chap. 7), the rise-time requirements are significantly relaxed to 320 ns.

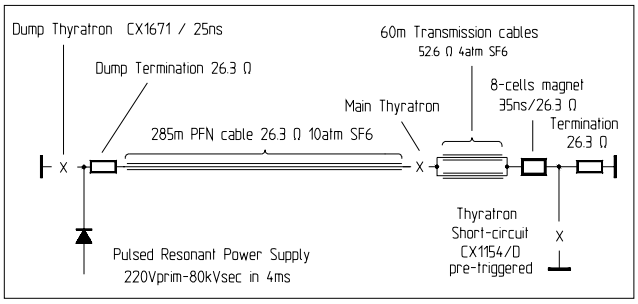

Figure 5.14: PS injection kicker KFA45 (1 of 4 modules).

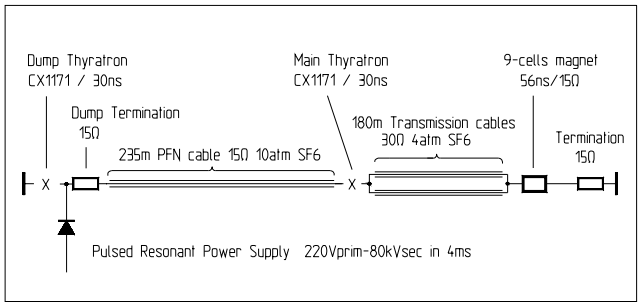

Figure 5.15: PS ejection kicker KFA71-79 (1 of 12 modules).

5.4 MORE POWERFUL WATER AND AIR COOLING SYSTEMS FOR THE PSB

The elements of the PSB (mainly magnets and power supplies) are cooled with demineralised water, distributed in three separated circuits. While each circuit has a different inlet cooling water pressure, the temperatures are equal. Moreover, they have a common return circuit.

Operating the PSB at 1.4 GeV raises the power dissipation of the main magnets (dipoles and quadrupoles) by about 60% to a level which the old cooling system could not tackle.

The demineralised water was circulating in a closed loop and cooled in heat exchangers whose primary coolant was industrial town water, sent to the drain after use. To avoid this waste of precious resources, CERN has decided to gradually replace town water by closed-circuit water systems using atmospheric coolants (cooling towers). For these reasons, a complete renovation of the PSB water cooling and air conditioning systems was undertaken (see Tab 5.4 for the system's key parameters).

Table 5.4: PSB water cooling system, old and new: key parameters.

	Old system			**New system**	
Installed cooling power [MW]	4			5.2	
Demineralised water circuit	Ring	Techn. Areas	Exp. Zones	Ring + Techn. Areas and TT2	Exp. Zones
Flow rate [m^3/h]	90	57	22	270	35
Max. inlet temperature [°C]	20	20	20	27	27
Inlet pressure on magnets [bar]	10.5	10	18	13	14.7
Outlet pressure on magnets [bar]	5	5	6	4.4	3.7
Press. difference available [bar]	5.5 [1]	5	12	8.6 [1]	11
Primary water circuit	Town water to drain			Water recycled via cooling towers	
Total flow rate [m^3/h]	120			465	
Average temperature [°C]	13			24	
Water pressure [bar]	6			2.5	
Replacement town water [m^3/h]	-			20	

[1] The higher pressure difference on the magnets copes with the increased power dissipation at 1.4 GeV.

The upgrading of the demineralised PSB water cooling system as shown in Fig. 5.16 implied:

- Concentration of all system components in a new building (237).
- Construction of a closed-circuit cooling plant based on cooling towers.
- Increase of the installed cooling power from 4 to 5.2 MW.
- Matching of the cooling requirements to just one single demineralised water supply with common temperature and pressure.
- Installation of a new device to generate demineralised water in the adjacent building (141), with a capacity of 6 m^3/h, aiming at a water conductivity below 2 μS. It is based on reverse osmosis

and no longer requires periodic in-situ regeneration of chemical products, except for the final ion exchangers.

It should be noted that the primary water temperature of the new system is subject to seasonal changes of the atmospheric coolant (air temperature, humidity), with concomitant variations of the PSB magnet temperature of up to 7□C. An extensive Machine Development (MD) session in July 1996 demonstrated that this temperature increase does not impair the PSB machine performance [13] at all.

The previous air conditioning system, with an installed power of 1.8 MW, was also adapted to atmospheric coolants, thus saving further 90 m^3/h of town water (Tab. 5.5). The new device was also installed in building 237.

Table 5.5: PSB air cooling system, before and after upgrading.

	Old system	**New system**
Installed cooling power [MW]	1.8	3
Primary water circuit		
Flow rate [m^3/h]	100	258
Average temperature [°C]	13	24
Town water consumption [m^3/h]	100 (to drain)	10 (replacement)
Saving in town water consumption [m^3/h]		90

More detailed information on this upgrading programme may be found in [14]. The overall saving in town water consumption (both systems) amounts to 190 m^3/h. The renovated systems became operational for the accelerator start-up in March 2000.

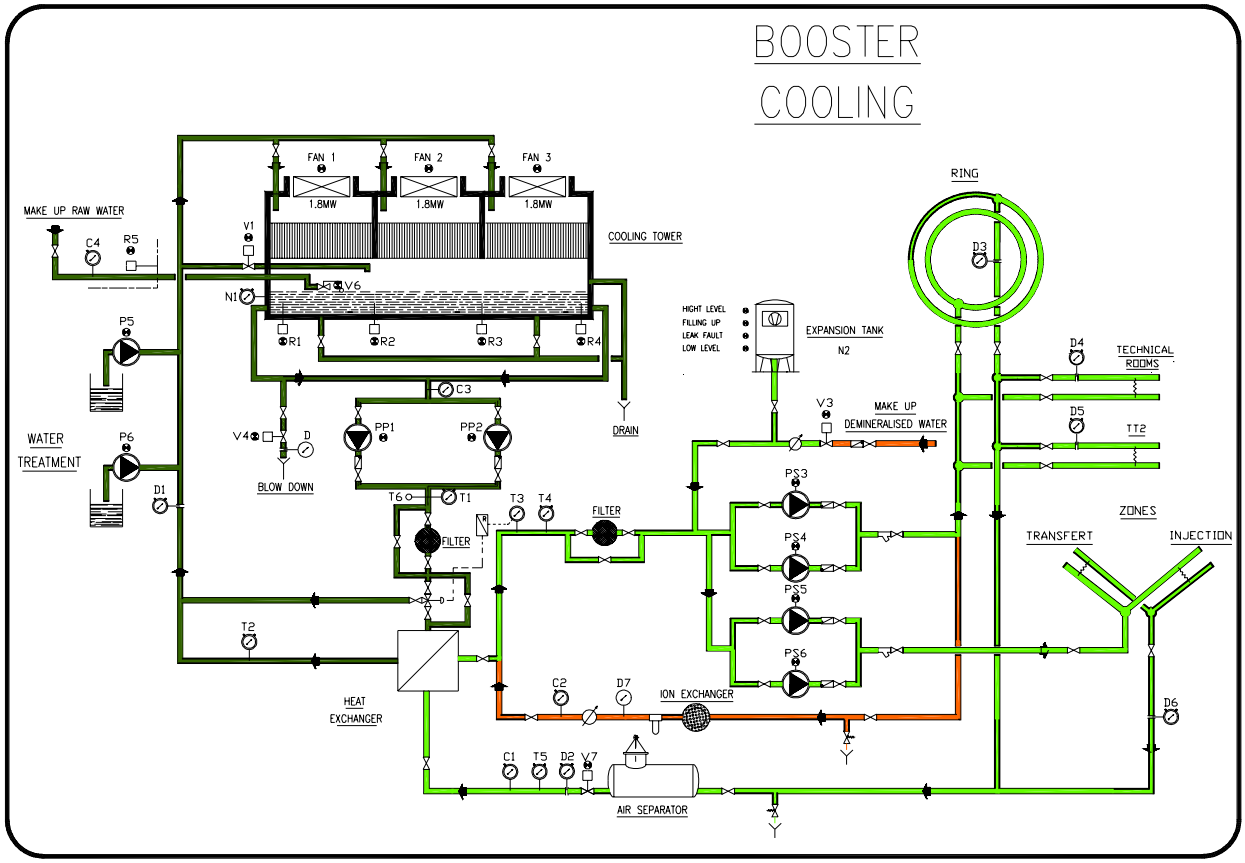

Figure 5.16: Demineralised water cooling system of the PSB after upgrading in March 2000.

REFERENCES

[1] J. Borburgh, M. Hourican, M. Thievent, *A new set of magnetic septa in the CERN PS Complex,* Proc. PAC '99, New York, 1999.

[2] G.S. Clark, A.J. Otter, P. Reeve, *Magnets for the CERN PS Booster transfer line,* Proc. PAC '97, Vancouver, 1997.

[3] M.J. Barnes et al., *New Magnets for the transfer line PSB-CPS,* CERN SL-Note-98-052 MS, Geneva, 1998.

[4] D. Evans, M.J. Barnes, B. Evans, R. Nussbaumer, *Rotating coil and data acquisition system for measuring CERN beam transferline quadrupole magnets,* Proc. of IMMW 10, Batavia, Illinois, 1999.

[5] M.J. Barnes, G.S. Clark, M. Sassowsky, *Three dimensional field calculations compared to magnetic measurements for CERN PSB-CPS transfer line magnets,* Proc. PAC '99, New York, 1999.

[6] A. Brückner, *Kicking protons, fast and cheap*, 1971 US Particle Accelerator Conf., Chicago, 1971.

[7] A. Brückner, *A non-linear step-pulse steepening delay line*, CERN Report 68-25, Geneva, 1968.

[8] K.D. Metzmacher, L. Sermeus, *The PSB Ejection and Recombination Kicker Systems for LHC*, PS/CA/Note 2000-004, Geneva, 2000.

[9] A. Fowler, *The PSB ejection bumper system for LHC*, CERN PS-CA Note 99-22, Geneva, 1999.

[10] K.D. Metzmacher, L. Sermeus, *The PS Injection Kicker KFA45 Performance for LHC,* PS/PO/Note 2002-015 (Tech.), Geneva, 2002.

[11] M. Benedikt (editor), *The PS Complex as Proton Pre Injector for the LHC – Design and Implementation Report,* CERN 2000-003, Geneva, 2000.

[12] K.D. Metzmacher, L. Sermeus, *The PS Ejection Kicker KFA71-79 Performance for LHC,* PS/PO/Note 2001-057 (Tech.), Geneva, 2001.

[13] B. Dumas et al., *PSB ME 10.-19.7.1996: Cooling water in tunnel* $+7^0$C, PS/HI/Note 96-10 (ME), Geneva, 1996.

[14] W. Van Cauter, *Adaptation des systèmes de refroidissement et climatisation du Booster en vue du LHC*, CERN ST-CV/96.061/WVC/bm, Geneva, 1996.